C$_5$–C$_7$ linear alkane hydroisomerization over MoO$_3$–ZrO$_2$ and Pt/MoO$_3$–ZrO$_2$ catalysts

S. Triwahyono [a,b,*], A.A. Jalil [c], N.N. Ruslan [a], H.D. Setiabudi [c], N.H.N. Kamarudin [c]

[a] Department of Chemistry, Faculty of Science, Universiti Teknologi Malaysia, 81310 UTM Johor Bahru, Malaysia
[b] Ibnu Sina Institute for Fundamental Science Studies, Universiti Teknologi Malaysia, 81310 UTM Johor Bahru, Malaysia
[c] Institute of Hydrogen Economy, Faculty of Chemical Engineering, Universiti Teknologi Malaysia, 81310 UTM Johor Bahru, Malaysia

ARTICLE INFO

ABSTRACT

The catalytic activity of MoO$_3$–ZrO$_2$ and Pt/MoO$_3$–ZrO$_2$ has been assessed based on the C$_5$–C$_7$ linear alkane hydroisomerization in a microcatalytic pulse reactor at 323–623 K. The introduction of Pt altered the crystallinity and acidity of MoO$_3$–ZrO$_2$. The catalytic activity of Pt/MoO$_3$–ZrO$_2$ was inferior than that of MoO$_3$–ZrO$_2$, although the Pt/MoO$_3$–ZrO$_2$ performed higher hydrogen uptake capacity. IR and ESR studies confirmed the heating of MoO$_3$–ZrO$_2$ in the presence of hydrogen formed active protonic acid sites and electrons which led to change in the Mo oxidation state. Similar phenomenon was observed for Pt/MoO$_3$–ZrO$_2$ at ⩽323 K. Contrarily, heating of Pt/MoO$_3$–ZrO$_2$ in the presence of hydrogen at higher temperature did not form protonic acid sites but intensified Lewis acidic sites. It is suggested that Pt facilitates in the interaction of spiltover hydrogen atom and MoO$_3$ to form MoO$_2$ or Mo$_2$O$_5$ over ZrO$_2$ support which may be intensified the Lewis acidic sites.

1. Introduction

The isomerization of linear alkanes over solid acid catalysts has received great attention as an environmentally safety way to improve the octane number of gasoline in recent year [1–5]. Zeolite and chlorided alumina-based catalysts have been studied extensively in the linear alkane isomerization for industrial purposes; however, they have some disadvantages such as relatively low activity and tolerance to the impurities which lead to decrease the yield of isomer products [6]. Recently, the use of transition metal-loaded catalysts has drawn much attention due to their ability to isomerize C$_4$–C$_7$ linear alkane effectively. In addition, the presence of noble metals such as Pt or Pd in zeolitic materials, chlorided alumina, and zirconia-based catalysts is widely reported to improve the stability and activity of the catalysts [7–15]. The Pt has a role in the formation of active protonic acid sites and/or assisting in the removal of coke deposits through hydrogenation processes. Iglesia and co-workers reported the roles of Pt and hydrogen on WO$_3$–ZrO$_2$ catalyst in the n-heptane isomerization in which they concluded that Pt/WO$_3$–ZrO$_2$ showed a higher activity than that of Pt/SO$_4^{2-}$–ZrO$_2$ due to the availability of hydrogen on the surface of WO$_3$–ZrO$_2$ to suppress cracking process [16,17].

Recently, a special interest was devoted to molybdenum oxide promoted zirconia (MoO$_3$–ZrO$_2$) in the catalysis. Afanasiev studied the preparation of MoO$_3$/ZrO$_2$ in which the metastable monolayer coverage of zirconia surface can be obtained by solid–solid wetting preparation method with the Mo/Zr ratio of 0.13–0.15 [18]. While, Calafat et al. reported the effect of Mo/Zr ratio and digestion time in the physical properties of MoO$_3$/ZrO$_2$ [19]. The surface area of MoO$_3$/ZrO$_2$ was increased with the increasing Mo/Zr ratio and decreased with the increasing the digestion time. In addition, they also have suggested that the addition of (NH$_4$)$_6$Mo$_7$O$_{24}$ after formation of the Zr(OH)$_4$ gel results in an increase in surface area than those obtained by co-precipitation. Xie et al. studied the crystalline structure in MoO$_x$/ZrO$_2$ evidenced by X-ray absorption and Raman spectroscopy in which the isolated tetrahedral MoO$_x$ species was observed at low surface density (<5 Mo/nm^2) of sample treated at 873 K and below [20]. For MoO$_x$/ZrO$_2$ samples with higher surface density (>5 Mo/nm^2), treatment in air at 723 K led to the predominant formation of MoO$_3$, while higher treatment temperatures led to a solid-state reaction between MoO$_3$ and ZrO$_2$ to form Zr(MoO$_4$)$_2$. Meanwhile, the effect of Mo loading on ZrO$_2$ in respect to the catalytic activities was reported by Chary et al. [21] and Kenney et al. [22]. Chary et al. demonstrated the catalytic ammoxidation of toluene to benzonitrile over MoO$_3$–ZrO$_2$ increased with loading up to 6.6 wt.% MoO$_3$. They have also claimed that the theoretical monolayer loading of MoO$_3$ on the ZrO$_2$ was obtained at 6.6 wt.% MoO$_3$ loading in which this monolayer MoO$_3$ on ZrO$_2$ resulted to the strongest acidity and highest reducibility of the

MoO$_3$/ZrO$_2$ catalyst, whereas Kenney et al. reported the influence of Mo loading on ZrO$_2$ in the methylcyclopentane conversion. They have concluded that the most active catalyst for methylcyclopentane conversion corresponds to a molybdenum loading of 3.2 at.% Mo, which has the highest acidity per surface area of the ZrO$_2$–MoO$_3$ catalysts studied. In addition, the surface area of ZrO$_2$–MoO$_3$ reached a maximum value of 124 m^2/g at a loading of 15.8 at.% Mo, while the isothermal CO$_2$ adsorption and ammonia TPD results indicated the strength of basic sites and specific NH$_3$ desorption decreased with increasing molybdenum content.

We have previously reported the acidic properties of MoO$_3$–ZrO$_2$, in relation to the active sites which participate in the formation of active protonic acid sites from molecular hydrogen that favor in n-heptane isomerization [23,24]. Although it has also been reported widely that the introduction of Pt site is able to improve the activity and stability of zeolites, alumina, WO$_3$–ZrO$_2$, and SO$_4^{2-}$–ZrO$_2$, there is almost no report related to the study of Pt loaded on MoO$_3$–ZrO$_2$ for hydroisomerization of alkanes in the literature. In this study, we explored the effects of Pt in the properties and activity of MoO$_3$–ZrO$_2$. The MoO$_3$–ZrO$_2$ with and without Pt were examined in the hydroisomerization of n-pentane, n-hexane, and n-heptane, whereas the interaction of molecular hydrogen and surface catalyst was observed by quantitative hydrogen adsorption measurement, IR and ESR spectroscopy. We found that the presence of Pt did not enhance the activity of MoO$_3$–ZrO$_2$ in the hydroisomerization of n-alkanes, although the Pt enhanced the hydrogen uptake capacity of MoO$_3$–ZrO$_2$. IR and ESR studies revealed that the presence of Pt did not promote the formation of protonic acid sites from molecular hydrogen. In contrast, the presence of Pt intensified the Lewis acid sites in which this may correspond to presence of MoO$_2$ or Mo$_2$O$_5$ species on the surface of ZrO$_2$.

2. Experimental

2.1. Catalyst preparation

Zirconium hydroxide (Zr(OH)$_4$) was prepared from aqueous solution of ZrOCl$_2$·8H$_2$O (Wako Pure Chemical) by hydrolysis with 2.5% NH$_4$OH (Merck) aqueous solution [25]. The final pH of solution was 9.0. The product was decanted and filtered, followed by drying at 383 K overnight to form zirconium hydroxide. The MoO$_3$–ZrO$_2$ sample was prepared by impregnation of zirconium hydroxide with aqueous solution of ammonium heptamolybdate ([NH$_4$]$_6$Mo$_7$O$_{24}$·4H$_2$O, Merck), followed by drying at 383 K and calcination at 1093 K in air. The surface area of MoO$_3$–ZrO$_2$ was 56 m^2/g, and the content of Mo was 5 wt.%. The Pt/MoO$_3$–ZrO$_2$ sample was prepared by impregnation of the MoO$_3$–ZrO$_2$ with an aqueous solution of hexachloroplatinic acid (H$_2$PtCl$_6$·H$_2$O, Wako Pure Chemical) followed by calcination at 823 K in air. The surface area was 54 m^2/g, and the content of Pt and Mo was 0.5 and 4.7 wt.%, respectively.

2.2. Characterization of catalyst

The crystalline structure of catalysts was determined with X-ray diffraction (XRD) recorded on a Bruker AXS D8 Automatic Powder Diffractometer using Cu Kα radiation with λ = 1.5418 Å at 40 kV and 40 mA over a range of 2θ = 20–80°. The fraction of the tetragonal phase of zirconia in the sample was determined based on the formula proposed by Toraya et al. [26]. The XRD measurement of H$_2$-reduced sample was determined as follows: Sample was reduced with H$_2$ at 673 K for 3, 6, and 12 h. After cooling to room temperature under H$_2$ atmosphere, the reduced sample was transferred to a glove box without exposure to air then dispersed in a solution of heptane to avoid any bulk oxidation.

The nitrogen adsorption–desorption isotherms was determined with a Quantachrome Autosorb-1 at 77 K. Prior to measurement, the samples were outgassed at 573 K for 3 h. The specific surface areas of the samples were determined from the linear portion of the BET plots. Pore size distribution was calculated from the desorption branch of N$_2$ adsorption–desorption isotherm using the conventional Barret–Joyner–Halenda (BJH) method, while the metal content on the catalyst was measured with Agilent 4100 Microwave Plasma – Atomic Emission Spectrometer.

In the measurement of IR spectra, a self-supported wafer was placed in an in situ stainless steel IR cell with CaF$_2$ windows and outgassed at 623 K for 3 h. For pyridine adsorption measurement, 2 Torr of pyridine was adsorbed on activated samples at 423 K for 30 min followed by outgassing at 573 K for 30 min [11]. In the H$_2$-exposure experiments, the sample was exposed to 6.7 kPa of hydrogen at room temperature to 473 K in 50 K increments. All spectra were recorded on an Agilent Cary 640 FTIR Spectrometer at room temperature. The intensity of acidic sites was determined by Gaussian curve fitting method.

The ESR measurement was carried out in a JEOL JES-FA100 ESR spectrometer, to observe the formation of unpaired electrons in vacuo heating and to observe the interaction of the unpaired electrons with electrons formed from molecular hydrogen at room temperature to 473 K [27]. The catalyst was outgassed at 623 K for 3 h followed by the introduction of 6.7 kPa of hydrogen gas at room temperature. Then, the catalyst was held at room temperature and heated at 323, 373, 423, and 473 K in the presence of hydrogen gas. All signals were recorded at room temperature.

The hydrogen uptake capacity of catalysts was measured using the automatic gas adsorption apparatus Belsorp-28SA. A catalyst sample was placed in an adsorption vessel and activated in a hydrogen flow at 623 K for 3 h followed by evacuation at 623 K for 3 h. The sample was subsequently cooled to an adsorption temperature and held for 3 h in order to stabilize the temperature [28]. The adsorption temperature was verified from 323 to 573 K. 6.7 kPa of hydrogen gas was then introduced into the adsorption system, and the pressure change was monitored to calculate the hydrogen uptake.

2.3. Hydroisomerization of n-alkane

The hydroisomerization of n-pentane, n-hexane, and n-heptane was performed under hydrogen atmosphere in a microcatalytic pulse reactor at temperature range of 423–623 K. Prior to the reaction, the catalyst was activated in an oxygen stream (F_{Oxygen} = 100 mL/min) at 623 K for 1 h, followed by heated in a hydrogen stream ($F_{Hydrogen}$ = 100 mL/min) at 623 K for 3 h, and then cooled to a reaction temperature in a hydrogen stream. A dose of n-alkane (n-pentane = 43 μmol, n-hexane = 38 μmol, n-heptane = 34 μmol) was passed over the 0.4 g of activated catalyst in a hydrogen stream ($F_{Hydrogen}$ = 100 mL/min), and the products were trapped at 77 K before being flash-evaporated into an online 6090 N Agilent gas chromatograph equipped with a VZ-7 packed column and an FID detector. Since all catalysts reached steady-state condition within seven pulses (280 min), results at seven pulses were used.

The specific rate of reactant conversion (r) from the differential conversion data was determined by the following equation:

$$r(\mu mol/(s\,m^2 cat)) = k\frac{\sum[C]_i - [C]_{residual\_reactant}}{\sum[C]_i} \qquad (1)$$

where $[C]_i$ and $[C]_{residual\_reactant}$ are mol number for particular product and for residual reactant, which was calculated based on the Scott hydrocarbon calibration standard gas (Air Liquide America Specialty Gases LLC). The rate constant (k) was determined by the molar concentration of the reactant divided by the surface area of

catalyst per unit time, with the assumption that the retention time for reactant in the catalyst bed was negligibly small. The calculated k values of n-pentane, n-hexane, and n-heptane for MoO$_3$–ZrO$_2$ were 1.94, 1.70, and 1.51 μmol/(s m^{2}cat), respectively, while the calculated k values of n-pentane, n-hexane, and n-heptane for Pt/MoO$_3$–ZrO$_2$ were 2.01, 1.76, and 1.57 μmol/(s m^{2}cat), respectively.

The selectivity (S_i) and yield (Y_i) to particular product was calculated according to following equations:

$$S_i(\%) = \frac{[C]_i}{\sum[C]_i - [C]_{reactant}} \times 100 \tag{2}$$

$$Y_i(\%) = S_i\frac{r}{k} \tag{3}$$

3. Results and discussion

3.1. Properties of Pt/MoO$_3$–ZrO$_2$

Fig. 1A shows the XRD pattern of MoO$_3$–ZrO$_2$ and Pt/MoO$_3$–ZrO$_2$, respectively. MoO$_3$–ZrO$_2$ exhibited three well-established polymorphs: the monoclinic, tetragonal, and cubic phase of ZrO$_2$. The sharp diffraction lines at 2θ = 17.3°, 28.2°, 31.5°, 33.9°, 38.4°, 40.6°, 44.5°, 50.1°, and 55.3° correspond to the monoclinic phase of ZrO$_2$, peaks at 2θ = 30.2°, 34.3°, 49.1°, 59.7°, and 62.6° correspond to the tetragonal phase of ZrO$_2$, while the peaks at 2θ = 32.9° and 70.4° correspond to cubic phase of ZrO$_2$. A small peak was observed at 2θ = 23.9° which may be related to the presence of Zr(MoO$_4$)$_2$ hexagonal phase [23,29]. No intensity corresponds to the reflections of Pt (1 1 1), which should appear at 2θ = 40°, was observed in the XRD pattern of Pt/MoO$_3$–ZrO$_2$. This suggested that the quantity of Pt loading was small and therefore finely dispersed on the surface or below the XRD detection limit. The introduction of Pt changed slightly the crystallinity of ZrO$_2$. The fraction of tetragonal phase of ZrO$_2$ decreased from 0.51 to 0.44 which may be due to the collapsing of crystalline phase during calcination. The decrease in the crystallinity may not be due to the altering of Mo loading. In fact, MP-AES results indicated that the

Mo loading was 5 and 4.7 wt.% for MoO$_3$–ZrO$_2$ with and without Pt. In addition, the specific surface area altered slightly from 56 to 54 m^2/g. Fig. 1B shows the XRD patterns of Pt/MoO$_3$–ZrO$_2$ reduced with H$_2$ at 673 K for 3, 6, and 12 h. There were no significant changes on the H$_2$-reduced Pt/MoO$_3$–ZrO$_2$. This may be due to the amount of Mo loading was very small compared to the ZrO$_2$ support.

The N$_2$ adsorption–desorption isotherms and pore size distribution for MoO$_3$–ZrO$_2$ and Pt/MoO$_3$–ZrO$_2$ are plotted in Fig. 2A and B, respectively. The introduction of Pt did not much alter the N$_2$ physisorption results. The N$_2$ adsorption–desorption isotherms can be classified as a type IV isotherm for both catalysts, with the pore filling restricted to a range of P/P_o = 0.55–0.8, typical of mesoporous materials. According to IUPAC classification, the hysteresis loop is type H2 indicating a complex mesoporous structure. This type of hysteresis is characteristic of solids consisting of particles crossed by nearly cylindrical channel. The pore size distribution of samples was derived from the desorption branch of the N$_2$ adsorption–desorption isotherm, shown in Fig. 2B. Both samples exhibited narrow pore size distribution and sharp pore distribution peak with pore diameter of 5 nm. The peak at 5 nm decreased slightly after the introduction of Pt on MoO$_3$–ZrO$_2$, indicating some Pt particles plugged into the pore of MoO$_3$–ZrO$_2$ which led to decrease the specific surface area of ZrO$_2$.

3.2. Intrinsic acidity

The type of acid sites for MoO$_3$–ZrO$_2$ and Pt/MoO$_3$–ZrO$_2$ was qualitatively probed by pyridine adsorption using IR spectroscopy [30]. Fig. 3A shows the IR spectra of pyridine adsorbed on MoO$_3$–ZrO$_2$ and Pt/MoO$_3$–ZrO$_2$ activated at different temperatures. The catalysts were activated at 573, 623, and 673 K for 3 h, the spectra were recorded after the adsorption of pyridine on samples reach equilibrium at 423 K, and the physisorbed state was subsequently removed by heating at 573 K under vacuum. Thus, the resulting absorbance bands indicated only strong adsorptions between the pyridine molecules and acidic sites. Typical Brønsted acid sites
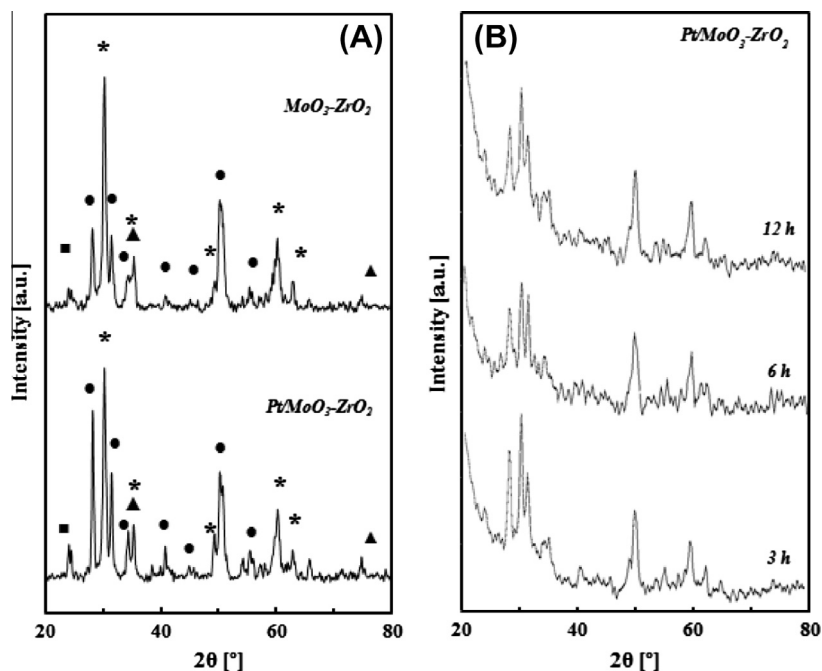

Fig. 1. (A) X-ray diffraction patterns of MoO$_3$–ZrO$_2$ and Pt/MoO$_3$–ZrO$_2$. (●) Monoclinic phase of ZrO$_2$; (*) tetragonal phase of ZrO$_2$; (▲) cubic phase of ZrO$_2$; (■) Zr(MoO$_4$)$_2$ phase. (B) X-ray diffraction patterns of Pt/MoO$_3$–ZrO$_2$ reduced with H$_2$ at 673 K for 3, 6 and 12 h.
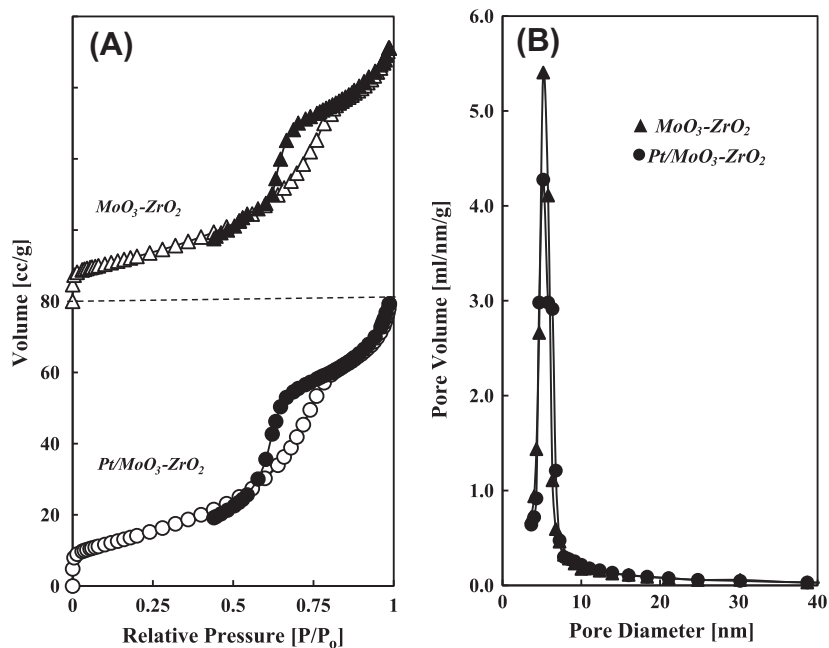
Fig. 2. (A) Adsorption–desorption isotherms of N_2 on MoO_3–ZrO_2 and Pt/MoO_3–ZrO_2. Open and solid symbols represent adsorption and desorption isotherms, respectively. (B) Pore size distribution of MoO_3–ZrO_2 and Pt/MoO_3–ZrO_2.
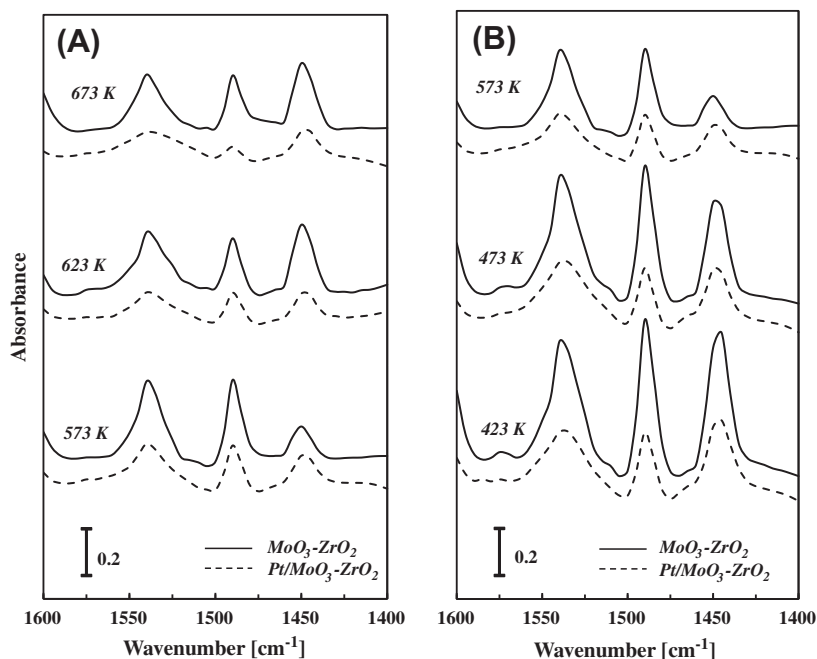

Fig. 3. (A) IR spectra of pyridine adsorbed on MoO_3–ZrO_2 and Pt/MoO_3–ZrO_2 samples activated at different temperatures. Pyridine was adsorbed at 423 K and outgassed at 573 K. (B) IR spectra of pyridine adsorbed on MoO_3–ZrO_2 and Pt/MoO_3–ZrO_2 at 423 K and outgassed at different temperatures. Samples were activated at 573 K.

were observed in the samples, suggesting that pyridine was adsorbed in the form of a pyridinium ion at the IR frequency of $1540\ cm^{-1}$, whereas strong Lewis electron pair acceptors were observed at $1450\ cm^{-1}$ in the samples. The absorbance band at $1490\ cm^{-1}$ corresponds to the mixture of Brønsted and Lewis acid sites. For MoO_3–ZrO_2 sample, as the activation temperature increased, the absorbance band at $1540\ cm^{-1}$ decreased and the other absorbance band at $1450\ cm^{-1}$ increased markedly due to the dehydration and/or dehydroxylation which eliminated acidic OH groups, leaving Lewis acid sites. This is commonly observed

for zeolites, mesoporous materials, and other mixed metal oxide such as silica–alumina and tungsten oxide–zirconium oxide. Meanwhile, different phenomenon was observed for Pt/MoO_3–ZrO_2. In general, the intensity of the absorbance bands attributed to both Brønsted and Lewis acid sites for Pt/MoO_3–ZrO_2 is lower than that of MoO_3–ZrO_2. The difference is not due to the amount of Mo, as both catalysts have almost similar Mo loading. However, this may be due to the small altering of the crystallinity of ZrO_2 during the calcination in which the tetragonal phase of zirconia decreased with Pt-addition. Increase in the activation temperature of

Pt/MoO$_3$–ZrO$_2$ decreased moderately the Brønsted acid sites, whereas the band ascribed to the Lewis acid sites did not change much significantly. These results indicated that MoO$_3$–ZrO$_2$ possessed several acidic OH groups with different strength in which the acidic OH groups were extensively eliminated at higher activation temperature leaving Lewis acid sites. Meanwhile, most of the acidic OH groups and Lewis acid sites were strong for Pt/MoO$_3$–ZrO$_2$. The weak to moderate strength of acidic OH groups was eliminated at relatively low activation temperature. Therefore, the change was not observed for both acidic sites on Pt/MoO$_3$–ZrO$_2$ with increasing the activation temperature. Fig. 3B shows the variations of the IR spectra as a function of outgassing temperature after pyridine adsorption for the sample activated at 573 K. If the outgassing temperature is raised, pyridine molecules adsorbed on weak acid sites should be desorbed at lower temperatures, and those adsorbed on strong acid sites should be desorbed at higher temperatures. For MoO$_3$–ZrO$_2$, both Brønsted and Lewis acid sites decreased significantly with outgassing temperature indicating the wide distribution of both acidic sites on the MoO$_3$–ZrO$_2$ sample [23]. It should be noted that the decrease was extensively observed for Lewis acid sites than that of Brønsted acid sites. This showed that most of the Brønsted acid sites on the MoO$_3$–ZrO$_2$ were strong. In addition to the strong Lewis acid sites, there existed weak acid sites for which the pyridine was desorbed at 423 K and above, whereas small decreased was observed for both acidic sites on Pt/MoO$_3$–ZrO$_2$, indicating the sample possesses small distribution of both acidic sites.

The properties of acidic sites on MoO$_3$–ZrO$_2$ types are essentially similar with WO$_3$–ZrO$_2$ types [31]. For both catalysts, Brønsted and Lewis acid sites were strong in which the pyridine molecules remain on both acid sites after outgassing at 573 K. In addition to strong Lewis acid sites, there existed a number of weak Lewis acid sites from which pyridine molecules were desorbed by outgassing at elevated temperature. While the Lewis acid sites were predominantly for WO$_3$–ZrO$_2$ types, the Brønsted acid sites were the most part for MoO$_3$–ZrO$_2$. The other difference between MoO$_3$–ZrO$_2$ and WO$_3$–ZrO$_2$ types was observed on the acidity of catalysts after the introduction of Pt. The presence of Pt did not change much the acidity for WO$_3$–ZrO$_2$ types, while the concentration of acidic sites was significantly reduced by the presence of Pt for MoO$_3$–ZrO$_2$ types. The intensity of Brønsted and Lewis acid sites for Pt/MoO$_3$–ZrO$_2$ did not change much by activation, and outgassing of pyridine indicating all the weak acid sites were eliminated by the presence of Pt. The other difference between MoO$_3$–ZrO$_2$ and WO$_3$–ZrO$_2$ types was observed in the distribution of Brønsted acid site. In addition to the strong Brønsted acid sites, MoO$_3$–ZrO$_2$ possesses significant number of weak Brønsted acid sites, whereas only strong Brønsted acid sites were observed on WO$_3$–ZrO$_2$ types.

3.3. Hydrogen interaction

The interaction of molecular hydrogen and surface MoO$_3$–ZrO$_2$ types was studied by hydrogen uptake measurement, pyridine pre-adsorbed IR and ESR spectroscopy in order to reveal the acidity induced by molecular hydrogen and the role of hydrogen in the activity of catalysts. Several research groups have reported the role of Pt metal and molecular hydrogen in the solid acid materials in which the presence of metal has affected positively in the acid-catalytic reaction under hydrogen stream. While the presence of Pt and molecular hydrogen has been reported to increase the stability and activity of catalysts due to the assisting of Pt to remove coke deposits on the surface catalyst by hydrogenation process [32–34], our research group has suggested that the presence of Pt facilitates the formation of active protonic acid sites for maintaining the activity and stability through hydrogen spillover phenomenon [35,36]. We have reported the formation of protonic acid sites through hydrogen spillover phenomenon evidenced by ESR and IR studies on the zeolitic-based and zirconia-based catalysts [31,36,37]. In addition, the presence of Pt enhanced the hydrogen uptake capacity of WO$_3$–ZrO$_2$ [35,38], SO$_4^{2-}$–ZrO$_2$ [39] and also MoO$_3$ [28] catalysts.

Fig. 4 shows the isothermal hydrogen adsorption for MoO$_3$–ZrO$_2$ type catalysts and effect of adsorption temperature in the hydrogen uptake capacity. The general features of hydrogen uptake for MoO$_3$–ZrO$_2$, SO$_4^{2-}$–ZrO$_2$, and WO$_3$–ZrO$_2$ types were essentially
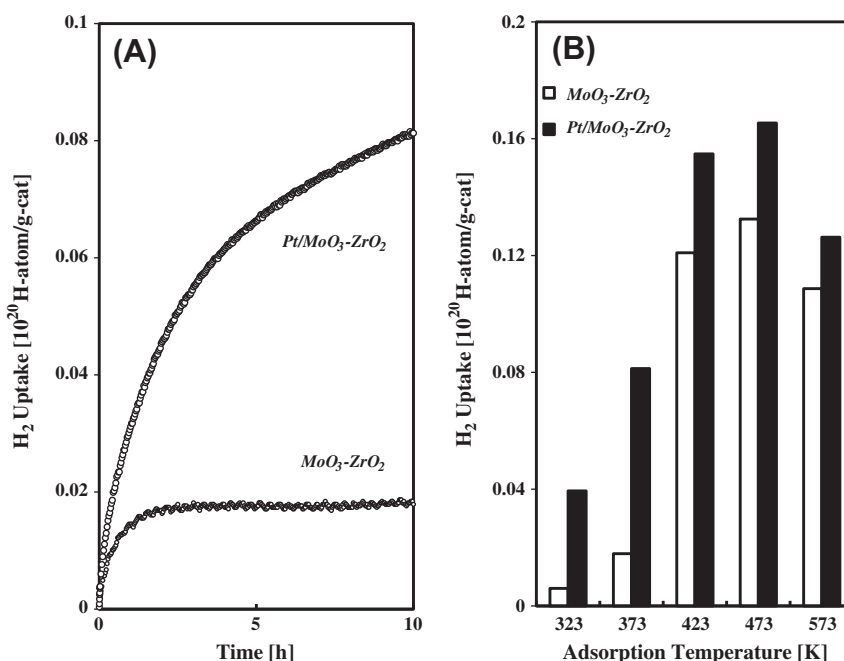
Fig. 4. (A) Hydrogen uptake on MoO$_3$–ZrO$_2$ and Pt/MoO$_3$–ZrO$_2$ as a function of time at 373 K. (B) Hydrogen uptake capacity of MoO$_3$–ZrO$_2$ and Pt/MoO$_3$–ZrO$_2$ at different adsorption temperatures after 10 h adsorption.
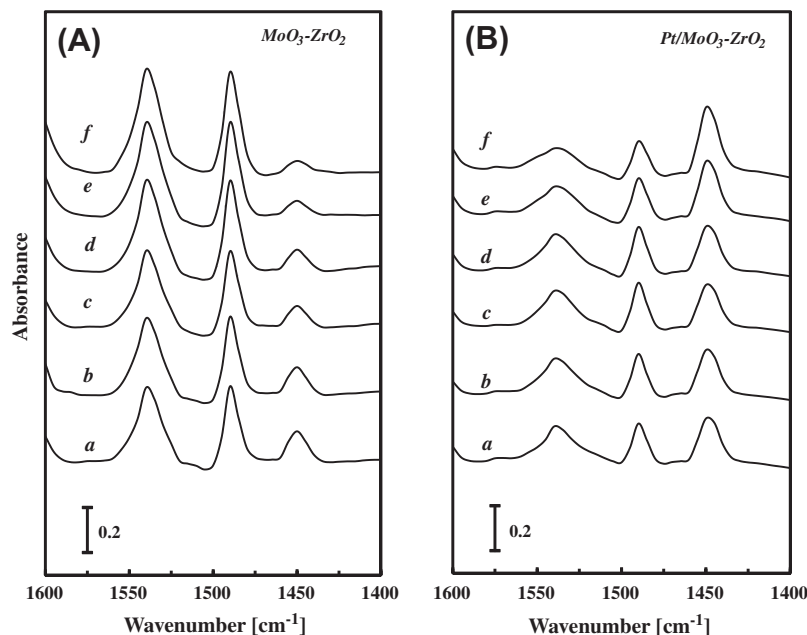
Fig. 5. IR spectra change of (A) MoO$_3$–ZrO$_2$ and (B) Pt/MoO$_3$–ZrO$_2$ when pyridine pre-adsorbed sample was heated in hydrogen at (b) room temperature, (c) 323 K, (d) 373 K, (e) 423 K and (f) 473 K. (a) Before exposure to hydrogen.

the same in which the presence of Pt enhanced the hydrogen up-take markedly [38,39]. For all adsorption temperatures, Pt loaded on SO$_4^{2-}$–ZrO$_2$ and WO$_3$–ZrO$_2$ performed fast adsorptions in the first few minutes followed by slower adsorption until equilibrium was reached. The decrease in the rate of hydrogen uptake with the time for both catalysts may be due to the decreasing of free Lewis acid sites for stabilizing of adsorbed hydrogen atoms by trapping of electrons. In the case of Pt/MoO$_3$–ZrO$_2$ catalyst, the presence of Pt continued the hydrogen uptake with time, and the adsorption did not reach equilibrium even after 10 h at 373 K. Different behaviors were observed for Pt-free MoO$_3$–ZrO$_2$ in which the hydrogen up-take increased to lesser extent with time and almost reached equi-librium within 3 h. For 10 h adsorption, the hydrogen uptake reached 8.13×10^{18} and 1.80×10^{18} H-atom/g cat for MoO$_3$–ZrO$_2$ with and without Pt at 373 K, respectively. This difference clearly verified that the presence of Pt facilitates the adsorption of hydro-gen on MoO$_3$–ZrO$_2$ catalyst for all adsorption temperatures as illustrated in Fig. 4B. In particular, the effect of Pt was obviously observed at 373 K and below due to the ability of Pt to interact with molecular hydrogen at relatively low temperature, while MoO$_3$–ZrO$_2$ began to interact with molecular hydrogen extensively at 423 K and above. This may indicate that Pt-free MoO$_3$–ZrO$_2$ pos-sess a higher energy barrier to be crossed over for hydrogen uptake than that of Pt/MoO$_3$–ZrO$_2$.

The interaction of hydrogen with the MoO$_3$–ZrO$_2$ type catalysts then was observed by IR and ESR spectroscopy (Figs. 5–7). We have previously reported the hydrogen spillover phenomenon over zirco-nia- and zeolite-based catalysts in which the molecular hydrogen dissociatively adsorbed on a specific site to form hydrogen atoms that undergo spillover onto the surface, followed by surface diffu-sion. Each spiltover hydrogen atom reaches a Lewis acid site and do-nates an electron to form an H$^+$. The H$^+$ is stabilized on an O atom near the Lewis acid site. The Lewis acid site trapping an electron re-acts with a second spiltover hydrogen to form an H$^-$ bound to a Lewis acid site [5,11]. The formation of protonic acid sites was mon-itored by IR spectroscopy, while the formation of electron was mon-itored by ESR spectroscopy [24,27]. Similar phenomenon was observed for MoO$_3$–ZrO$_2$ in which the interaction of hydrogen with the surface catalyst formed protonic acid sites and electrons which

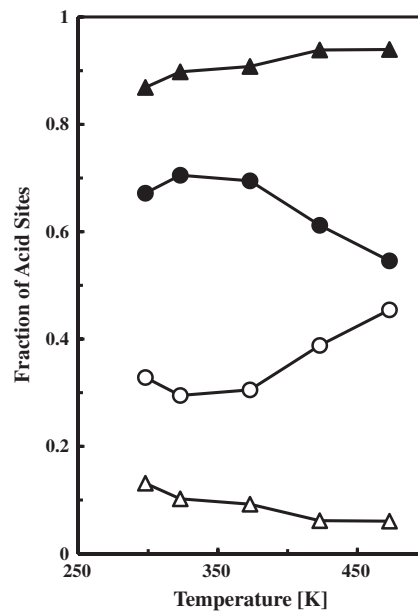**Fig. 6.** Plot of (▲,△) MoO$_3$–ZrO$_2$ and (●,○) Pt/MoO$_3$–ZrO$_2$ pre-adsorbed pyridine followed by heating in the presence of hydrogen. Solid symbol: Brønsted acid sites; open symbol: Lewis acid sites.

led to change in the Mo oxidation state. Heating in the presence of hydrogen, the absorbance band of acidic OH group at 1545 cm^{-1} was intensified indicating the formation of OH groups (Fig 5A), while the ESR signal at $g = 1.93$ corresponds to hexa-coordinated Mo^{5+} species decreased due to the increase in the interaction of electrons and electron-deficient Mo^{5+} cations (Fig. 7A inset) [24,40]. The changes were clearly seen in the Figs. 6 and 7B. The fraction of pro-tonic acid sites increased with increasing temperature and simulta-neously decreased in the fraction of Lewis acid sites, while the ESR signal at $g = 1.93$ decreased continuously with increasing the heat-ing temperature. These results strongly evidenced that the forma-tion of proton and electron from hydrogen atom increased extensively with increasing the temperature.
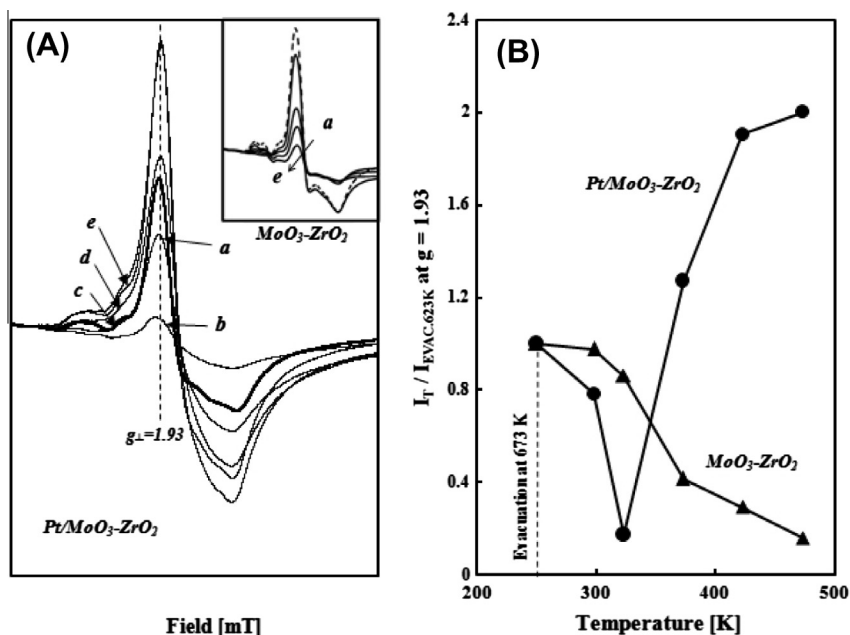
Fig. 7. (A) ESR spectra of Pt/MoO₃–ZrO₂ when 100 Torr of hydrogen was adsorbed at (a) room temperature, (b) 323 K, (c) 373 K, (d) 423 K and (e) 473 K. The sample was outgassed at 673 K (bold line) prior the hydrogen adsorption. Inset shows ESR spectra of MoO₃–ZrO₂. (B) Relative intensity of ESR spectra change for MoO₃–ZrO₂ and Pt/ MoO₃–ZrO₂ upon hydrogen adsorption.

Similar to SO_4^{2-}–ZrO_2 and WO_3–ZrO_2 type catalysts, the interaction of hydrogen with surface MoO_3–ZrO_2 is a reversible process in which the IR results indicated that the heating of the MoO_3–ZrO_2 in the presence of hydrogen gas altered the intensity of both Lewis and protonic acid sites (Fig. 6). while heating of the hydrogen adsorbed MoO_3–ZrO_2 in vacuum restored both Lewis and protonic acid sites to their original intensities (figure not shown). Differently, heating of the hydrogen adsorbed Pt/MoO_3–ZrO_2 in vacuum restored partially the intensity of both Lewis and protonic acid sites (figure not shown). The results also indicated that higher temperature is required to desorb the hydrogen uptake from the surface of Pt/MoO_3–ZrO_2.

In general, the presence of specific site likes Pt on solid acid catalyst is reported to increase the interaction of hydrogen and acidic surface which led to enhance the activity of catalyst in the acid-catalytic reaction. In this study, we are also reporting the hydrogen adsorption on MoO_3–ZrO_2 in which the presence of Pt increased the rate of hydrogen adsorption and hydrogen uptake capacity of MoO_3–ZrO_2. However, the hydrogen adsorbed IR and ESR studies on MoO_3–ZrO_2, indicating that the presence of Pt did not promote the formation of electron and active protonic acid sites such as $MoO_{2-x}(OH)_y$ phase or MoO_2–OH species at 373 K and above. In general, heating of Pt/MoO_3–ZrO_2 in the presence of hydrogen slightly decreased the Brønsted acid sites at 1545 cm^{-1} and increased gradually the Lewis acid sites at 1450 cm^{-1} (Fig. 5B). The changes of both Lewis and Brønsted acid sites caused by heating in the presence of hydrogen can be clearly seen when the fraction of absorbance bands at 1450 and 1545 cm^{-1} is plotted against the heating temperature (Fig. 6). Heating at 323 K and below, the Brønsted acid sites increased slightly with simultaneous decrease in the Lewis acid sites, indicating the formation of protonic acid sites from hydrogen atom. The further heating of Pt/MoO_3–ZrO_2 at 373 K, the Brønsted acid sites began to decrease and the decrease continued up to 473 K. In tandem, the intensity of Lewis acid sites increased at temperature range of 373–473 K. Similarly, the hydrogen adsorbed ESR spectroscopy showed that the signal at g = 1.93 decreased when the Pt/MoO_3–ZrO_2 was heating at 323 K and below (Fig. 7). This may be due to the interaction of

electron with electron-deficient Mo^{5+} cation. However, the heating at 373 K and above, ESR signal at g = 1.93 increased significantly indicating the increase in the number of electron-deficient Mo^{5+} cation and/or oxygen radical in the catalyst. The electron formed from hydrogen atom which subsequently pairing with electron-deficient Mo^{5+} cation and/or oxygen radical was not observed at 373 K and above. This result obviously indicated that Pt plays a different role on MoO_3–ZrO_2. The presence of Pt enhanced the interaction of hydrogen with the surface MoO_3–ZrO_2; however, the interacted-hydrogen did not successively form protonic acid sites but intensified the Lewis acid sites at >323 K.

Previously, Al-Kandari and co-workers have studied the interaction of hydrogen with MoO_3/TiO_2 catalysts [41–46]. They found that Mo_2O_5 species was most likely formed as an intermediate surface species in the reduction course of MoO_3 to MoO_2. All the molybdena species formed the surface Lewis acidity via exposed Mo^{6+} sites. Further exposure of the sample to hydrogen at 673 K for 12 h resulted in the formation of Brønsted (Mo–OH) acidic function on the surface of the MoO_2 structure, thereby producing a metal–acid (bifunctional) $MoO_{2-x}(OH)_y$ phase. Their results are quite similar to the results in this report on MoO_3–ZrO_2 type catalysts, although the formation of $MoO_{2-x}(OH)$ on both MoO_3–ZrO_2 and Pt/MoO_3–ZrO_2 was not observed by XRD results. However, the IR results suggested that the formation of protonic acid sites on MoO_3–ZrO_2 may be due to the presence of Mo–OH phase, while the formation of Lewis acid sites on Pt/MoO_3–ZrO_2 may be due to the presence of MoO_2 or Mo_2O_5 [41].

3.4. Hydroisomerization of n-pentane, n-hexane and n-heptane

Fig. 8 demonstrates the rate of conversion of MoO_3–ZrO_2 and Pt/ MoO_3–ZrO_2 in the C_5–C_7 linear alkane hydroisomerization at different temperatures. The results indicated that both catalysts were not active for n-pentane hydroisomerization at 323–573 K, in spite of trace amount of C_1–C_2 and C_3–C_4 cracking products was observed at 573 K and above. Meanwhile, both catalysts were active in n-hexane and n-heptane hydroisomerization. This result may be due to the dehydroisomerization and hydrocracking of n-pentane
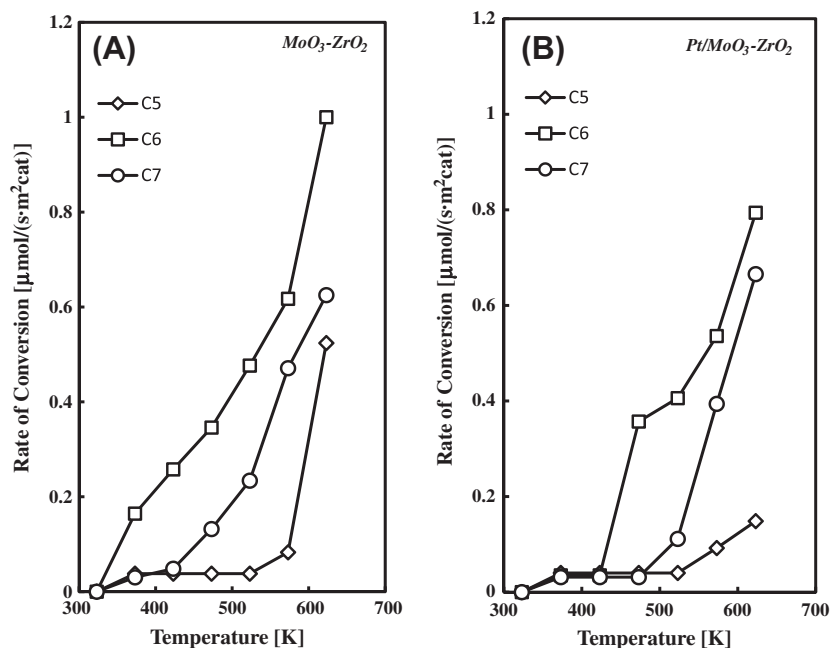
Fig. 8. Rate conversion for hydroisomerization of *n*-pentane, *n*-hexane and *n*-heptane at different reaction temperatures over (A) MoO₃–ZrO₂ and (B) Pt/MoO₃–ZrO₂.

Table 1
Product distribution of *n*-pentane, *n*-hexane and *n*-heptane isomerizations over MoO₃–ZrO₂ and Pt/MoO₃–ZrO₂ in the presence of hydrogen.

	MoO_3–ZrO_2							Pt/MoO_3–ZrO_2						
React. temp. (K)	323	373	423	473	523	573	623	323	373	423	473	523	573	623
n-pentane														
Rate of conversion (µmol/(s m²cat))	0	<0.04	<0.04	<0.04	<0.04	0.08	0.52	0	<0.04	<0.04	<0.04	<0.04	0.09	0.15
Selectivity (%)														
C_1–C_2	0	100	100	100	100	95.8	87.5	0	100	100	100	100	100	100
C_3–C_4	0	0	0	0	0	4.2	12.5	0	0	0	0	0	0	0
2-Methylbutane	0	0	0	0	0	0	0	0	0	0	0	0	0	0
Yield of *i*-C_5 (%)	0	0	0	0	0	0	0	0	0	0	0	0	0	0
n-hexane														
Rate of conversion (µmol/(s m²cat))	0	0.16	0.26	0.35	0.48	0.62	1.00	0	<0.04	<0.04	0.36	0.41	0.54	0.79
Selectivity (%)														
C_1–C_2	0	6.2	6.5	6.0	11.4	11.0	10.0	0	100	81.0	45.0	38.0	35.0	29.5
C_3–C_4	0	40.6	35.0	18.8	5.6	7.0	6.0	0	0	19.0	18.2	10.0	12.0	15.0
C_5	0	18.0	20.5	30.2	28.0	25.0	23.0	0	0	0	21.3	11.0	11.0	2.5
3-Methylpentane	0	24.3	25.0	25.0	35.5	38.3	45.7	0	0	0	12.5	25.0	25.2	38.4
2-Methylpentane	0	10.9	13.0	20.0	19.5	18.7	15.3	0	0	0	3.0	16.0	16.8	14.6
Yield of *i*-C_6 (%)	0	3.4	5.7	9.0	15.4	20.5	35.9	0	0	0	3.1	7.2	12.8	23.9
n-heptane														
Rate of conversion (µmol/(s m²cat))	0	<0.03	0.05	0.13	0.23	0.47	0.63	0	<0.03	<0.03	<0.03	0.11	0.39	0.67
Selectivity (%)														
C_1–C_2	0	100	96.0	28.0	13.6	13.3	16.2	0	100	100	100	100	83.0	55.0
C_3–C_4	0	0	4.0	26.0	13.5	15.0	15.0	0	0	0	0	0	17.0	24.0
C_5–C_6	0	0	0	32.8	45.2	27.0	36.0	0	0	0	0	0	0	12.0
2-Methylhexane	0	0	0	5.0	10.0	21.0	23.0	0	0	0	0	0	0	3.5
3-Methylhexane	0	0	0	8.0	17.0	22.0	23.8	0	0	0	0	0	0	5.5
3-Ethylpentane	0	0	0	0.2	0.7	1.7	1.2	0	0	0	0	0	0	0
Yield of *i*-C_7 (%)	0	0	0	1.1	4.2	13.8	19.7	0	0	0	0	0	0	3.8

are more difficult catalytic processes as compared to *n*-hexane and *n*-heptane [44]. Although the *n*-pentane hydroisomerization has been observed for MoO₃/TiO₂ catalyst [41–46], the presence of metallic function in balance with the acid function for MoO₃–ZrO₂ and Pt/MoO₃–ZrO₂ seems to be not in an optimized condition for the reaction to occur. High activity in *n*-hexane and *n*-heptane hydroisomerization was observed on MoO₃–ZrO₂ at 323–623 K and the yield increased continuously with reaction temperature. In contrast, Pt/MoO₃–ZrO₂ was active only in the *n*-hexane hydro-isomerization, though trace amount of several cracking products

was observed in the hydroisomerization of *n*-heptane over Pt/MoO₃–ZrO₂ at 573 K and above. The detail results were listed in Table 1.

Fig. 9 shows yield of isomer products for C₅–C₇ alkane hydroisomerization over MoO₃–ZrO₂ and Pt/MoO₃–ZrO₂. The yield of isopentane was nil for all reaction temperature over MoO₃–ZrO₂ and Pt/MoO₃–ZrO₂ catalysts, whereas the yield of isohexane and isoheptane varied with reaction temperature for both catalysts. Overall, the yield of isoproducts was higher for MoO₃–ZrO₂ than that of Pt/MoO₃–ZrO₂. In addition, the Pt/MoO₃–ZrO₂ was not
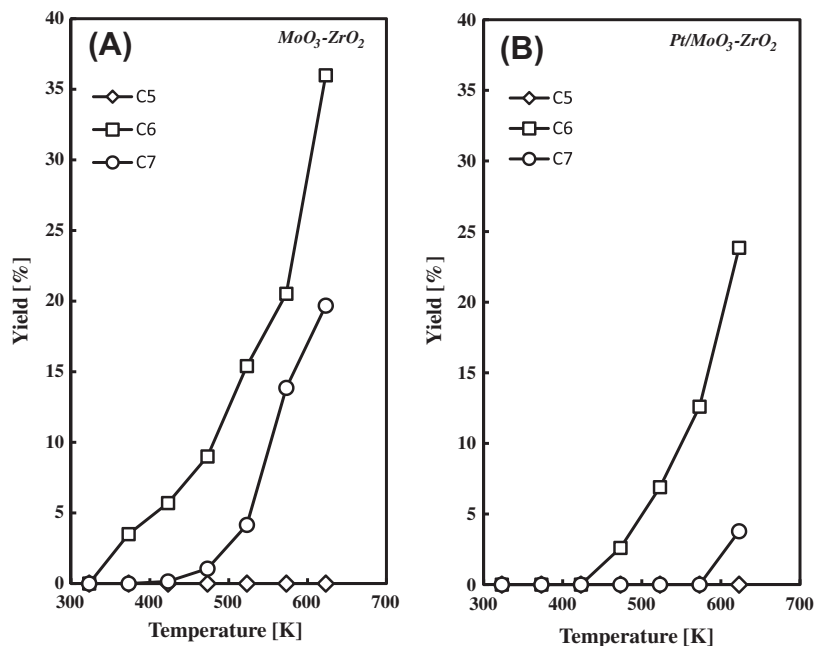
Fig. 9. Yield of isomer products for hydroisomerization of *n*-pentane, *n*-hexane and *n*-heptane at different reaction temperatures over (A) MoO₃–ZrO₂ and (B) Pt/MoO₃–ZrO₂.

active at low temperature. In fact, the yield for *n*-hexane and *n*-heptane hydroisomerization over Pt/MoO₃–ZrO₂ was observed only at >473 and >623 K, respectively. These results showed that the presence of Pt did not enhance the activity of MoO₃–ZrO₂ in *n*-pentane, *n*-hexane, and *n*-heptane hydroisomerization. In contrast, the presence of Pt has suppressed the selectivity of isoproducts and conversion of reactants. For instant, at 523 K, the yield of isohexane and isoheptane decreased by about 7% and 4%, respectively, whereas the rate of conversion of *n*-hexane and *n*-heptane were decreased by about 0.07 and 0.12 μmol/(s m²cat), respectively. Although it is not certain at present, the low activity of Pt/MoO₃–ZrO₂ may be caused by the Pt plays different role over MoO₃–ZrO₂ than those on the common catalysts such as WO₃–ZrO₂, SO₄²⁻–ZrO₂ or zeolite type catalysts. In the common solid acid catalysts, the presence of Pt facilitated the formation of active protonic acid sites from molecular hydrogen which finally enhanced the isomerization. However, IR and ESR results on Pt/MoO₃–ZrO₂ showed that the presence of Pt did not assist or enhance in the formation of protonic acid sites and electrons from molecular

hydrogen. The Pt on MoO₃–ZrO₂ may facilitate in the hydrogen uptake in which the hydrogen then interact with MoO₃ to form Mo with different oxidation state such as MoO₂ or Mo₂O₅ [41]. In fact, heating of Pt/MoO₃–ZrO₂ in the presence of hydrogen intensified the Lewis acid sites at 1450 cm⁻¹ in which the peak may correspond to the presence of Mo with different oxidation state on the surface of catalyst (Fig. 5). These results also confirmed that the activity of Pt/MoO₃–ZrO₂ could not be correlated directly to the hydrogen uptake capacity of the catalyst. The low activity of Pt/MoO₃–ZrO₂ was also observed on the isomerization of alkanes in the absence of hydrogen in which this suggested that the activity of Pt/MoO₃–ZrO₂ strongly depends on the active protonic acid sites originated from molecular hydrogen. Moreover, the low activity of Pt/MoO₃–ZrO₂ was not due to the low Mo loading or low concentration of permanent Brønsted acid sites.

Several research groups have reported the enhancement in the catalytic activity for platinum loaded on MoO₃-based catalysts. Al-Kandari and co-workers have studied the effects of Pt on the isomerization properties of MoO₃/TiO₂ catalyst [44–45]. They
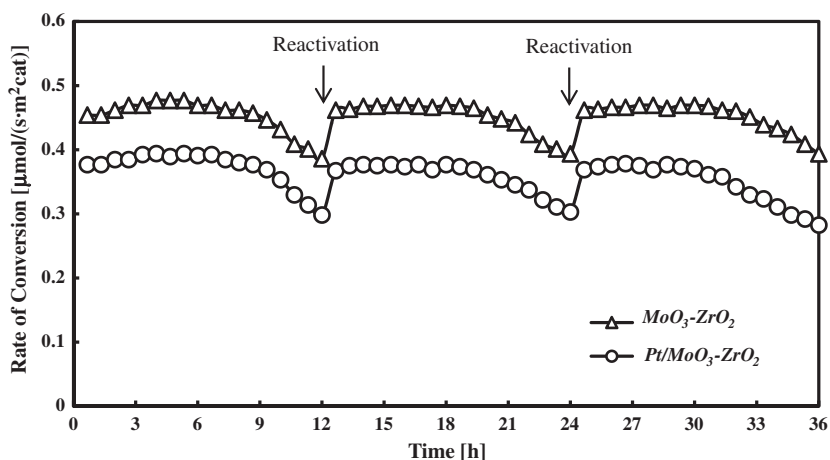

Fig. 10. Stability of MoO₃–ZrO₂ and Pt/MoO₃–ZrO₂ in the *n*-heptane hydroisomerization at 573 K. The reactivation was done under hydrogen stream at 623 K for 3 h. The intervals between each dose were kept constant at 40 min for more than 30 h.

found that the addition Pt on MoO₃/TiO₂ catalyst resulted in an increase in the catalytic activity of the system in favor of hydrocracking products at high reaction temperatures due to the enhancement in the metallic character of the system by metallic Pt(0), whereas Matsuda and co-workers have reported the effects of Pt on the catalytic activity of H_2-reduced MoO_3-based catalysts [47,48]. They found that H_2-reduced MoO_3 was almost inactive for heptane isomerization, while higher activity was obtained on H_2-reduced Pt/MoO_3. They suggested that the enhancement in the activity of H_2-reduced Pt/MoO_3 corresponds to the conversion of hydrogen molybdenum bronze, H_xMoO_3, to acidic molybdenum oxyhydride, MoO_xH_y. The MoO_xH_y species plays an important role in the generation of acid sites and led to the enhancement in the catalytic activities for heptane isomerization.

Fig. 10 shows the stability of MoO_3–ZrO_2 and Pt/MoO_3–ZrO_2 in the n-heptane hydroisomerization at 573 K. The reaction was done for more than 30 h with the intervals between each dose were kept constant at 40 min. The activity of the MoO_3–ZrO_2 and Pt/MoO_3–ZrO_2 reaches a steady-state condition within seven pulses (280 min) and decreased slightly after 12 pulses (480 min). However, the activity of the catalysts recovered after the activation in a hydrogen stream at 623 K for 3 h. It is noteworthy that the high activity of the MoO_3–ZrO_2 and Pt/MoO_3–ZrO_2 in the alkane hydroisomerization still has been observed after 30 h.

4. Conclusion

The introduction of Pt on MoO_3–ZrO_2 did not change much the crystallinity and BET specific surface area of MoO_3–ZrO_2 but altered significantly the concentration of acid sites of MoO_3–ZrO_2. Particularly, the presence of Pt partially eliminated strong permanent Brønsted and Lewis acid sites on MoO_3–ZrO_2. The alteration of the acidity is not due to the Mo loading, as both MoO_3–ZrO_2 and Pt/MoO_3–ZrO_2 have almost similar Mo loading. This alteration may be due to the small decrease in the crystallinity of ZrO_2 during the treatment. Interaction of molecular hydrogen with MoO_3–ZrO_2 showed the formation of protonic acid sites with simultaneous decrease in the Lewis acid sites through hydrogen spillover phenomenon in which the protonic acid sites act as active sites in n-hexane and n-heptane hydroisomerization. Contrarily, the presence of Pt on MoO_3–ZrO_2 lowered the catalytic activity of MoO_3–ZrO_2. Quantitative hydrogen adsorption, ESR and IR spectroscopy revealed that the presence of Pt enhanced the hydrogen adsorption rate and capacity of MoO_3–ZrO_2; however, the interacted-hydrogen did not successively form active protonic acid sites but intensified the Lewis acid sites. Therefore, the activity of Pt/MoO_3–ZrO_2 in the linear alkane isomerization is lower than that of MoO_3–ZrO_2 due to the inability of Pt to promote the formation of active protonic acid sites from molecular hydrogen on the surface of catalyst. In addition, the low activity of Pt/MoO_3–ZrO_2 was not due to the low Mo loading, as the Mo loading is almost similar for MoO_3–ZrO_2 with and without Pt. The low activity was also not due to the low concentration of permanent Brønsted acid sites in which the permanent Brønsted acid sites have no role in the isomerization.

References

[1] J.G. Santiesteban, D.C. Calabro, C.D. Chang, J.C. Vartulli, T.J. Fiebig, R.D. Bastian, J. Catal. 202 (2001) 25.
[2] M. Busto, V.M. Benitez, C.R. Vera, J.M. Grau, J.C. Yori, Appl. Catal. A: Gen. 347 (2008) 117.
[3] K. Kim, R. Ryoo, H. Jang, M. Choi, J. Catal. 288 (2012) 115.
[4] I.R. Choudhury, K. Hayasaka, J.W. Thybaut, C.S.L. Narasimhan, J.F. Denayer, J.A. Martens, G.B. Marin, J. Catal. 290 (2012) 165.
[5] H.D. Setiabudi, A.A. Jalil, S. Triwahyono, J. Catal. 294 (2012) 128.
[6] Y. Ono, Catal. Today 81 (2003) 3.
[7] A.H. Karim, S. Triwahyono, A.A. Jalil, H. Hattori, Appl. Catal. A: Gen. 433–434 (2012) 49.
[8] D. Fraenkel, N.R. Jentzsch, C.A. Starr, P.V. Nikrad, J. Catal. 274 (2010) 29.
[9] X. Zhu, L.L. Lobban, R.G. Mallinson, D.E. Resasco, J. Catal. 281 (2011) 21.
[10] N.H. N Kamarudin, A.A. Jalil, S. Triwahyono, R.R. Mukti, M.A.A. Aziz, H.D. Setiabudi, M.N.M. Muhid, H. Hamdan, Appl. Catal. A: Gen. 104 (2012) 431–432.
[11] S. Triwahyono, T. Yamada, H. Hattori, Catal. Lett. 85 (2003) 109.
[12] T.N. Vu, J. van Gestel, J.P. Gilson, C. Collet, J.P. Dath, J.C. Duchet, J. Catal. 231 (2005) 468.
[13] M. Occhiuzzi, D. Cordischi, S. De Rossi, G. Ferraris, D. Gazzoli, M. Valigi, Appl. Catal. A: Gen. 351 (2008) 29.
[14] S. Kuba, P. Lukinskas, R. Ahmad, F.C. Jentoft, R.K. Grasselli, B.C. Gates, H. Knözinger, J. Catal. 219 (2003) 376.
[15] X. Wang, H. Wang, Y. Liu, F. Liu, Y. Yu, H. He, J. Catal. 279 (2011) 301.
[16] D.G. Barton, S.L. Soled, G.D. Meitzner, G.A. Fuentes, E. Iglesia, J. Catal. 181 (1999) 57.
[17] E. Iglesia, D.C. Barton, S.L. Soled, S. Miseo, J.E. Baumgartner, W.E. Gates, G.A. Fuentes, G.D. Meitzner, Stud. Surf. Sci. Catal. 101 (1996) 533.
[18] P. Afanasiev, Mat. Chem. Phys. 47 (1997) 231.
[19] A. Calafat, L. Avilán, J. Aldana, Appl. Catal. A: Gen. 201 (2000) 215.
[20] S. Xie, K. Chen, A.T. Bell, E. Iglesia, J. Phys. Chem. B 104 (2000) 10059.
[21] K.V.R. Chary, K.R. Reddy, G. Kishan, J.W. Niemantsverdriet, G. Mestl, J. Catal. 226 (2004) 283.
[22] C. Kenney, Y. Maham, A.E. Nelson, Thermochim. Acta 434 (2005) 55.
[23] N.N. Ruslan, N.A. Fadzlillah, A.H. Karim, A.A. Jalil, S. Triwahyono, Appl. Catal. A: Gen. 406 (2011) 102.
[24] N.N. Ruslan, S. Triwahyono, A.A. Jalil, S.N. Timmiati, N.H.R. Annuar, Appl. Catal. A: Gen. 413–414 (2012) 176.
[25] S. Triwahyono, Z. Abdullah, A.A. Jalil, J. Nat. Gas. Chem. 15 (2006) 247.
[26] H. Toraya, S. Yoshimura, S. Somiya, J. Am. Ceram. Soc. 67 (1984) 119.
[27] M.A.A. Aziz, N.H.N. Kamarudin, H.D. Setiabudi, H. Hamdan, A.A. Jalil, S. Triwahyono, J. Nat. Gas Chem. 21 (2012) 29.
[28] S. Triwahyono, A.A. Jalil, S.N. Timmiati, N.N. Ruslan, H. Hattori, Appl. Catal. A: Gen. 372 (2010) 103.
[29] K. Chen, S. Xie, E. Iglesia, A.T. Bell, J. Catal. 189 (2000) 421.
[30] M. Tamura, K. Shimizu, A. Satsuma, Appl. Catal. A: Gen. 433–434 (2012) 135.
[31] S. Triwahyono, T. Yamada, H. Hattori, Appl. Catal. A: Gen. 242 (2003) 101.
[32] M.A. Alotaibi, E.F. Kozhevnikova, I.V. Kozhevnikov, J. Catal. 293 (2012) 141.
[33] M. Busto, C.R. Vera, J.M. Grau, Fuel Process. Technol. 92 (2011) 1675.
[34] P. Sun, G. Siddiqi, W.C. Vining, M. Chi, A.T. Bell, J. Catal. 282 (2012) 165.
[35] S. Triwahyono, A.A. Jalil, H. Hattori, J. Nat. Gas Chem. 16 (2007) 252.
[36] S. Triwahyono, A.A. Jalil, R.R. Mukti, M. Musthofa, N.A.M. Razali, M.A.A. Aziz, Appl. Catal. A: Gen. 407 (2011) 91.
[37] H.D. Setiabudi, S. Triwahyono, A.A. Jalil, N.H.N. Kamarudin, M.A.A. Aziz, J. Nat. Gas Chem. 20 (2011) 477.
[38] S. Triwahyono, T. Yamada, H. Hattori, Appl. Catal. A: Gen. 250 (2003) 65.
[39] N. Satoh, J.-i. Hayashi, H. Hattori, Appl. Catal. A: Gen. 202 (2000) 207.
[40] M. Occhiuzzi, D. Cordishi, R. Dragone, J. Phys. Chem. B 106 (2002) 12464.
[41] S. Al-Kandari, H. Al-Kandari, F. Al-Kharafi, A. Katrib, Appl. Catal. A: Gen. 341 (2008) 160.
[42] H. Al-Kandari, F. Al-Kharafi, A. Katrib, Appl. Catal. A: Gen. 361 (2009) 81.
[43] H. Al-Kandari, F. Al-Kharafi, A. Katrib, Appl. Catal. A: Gen. 383 (2010) 141.
[44] H. Al-Kandari, A.M. Mohamed, F. Al-Kharafi, A. Katrib, Catal. Commun. 12 (2011) 1188.
[45] H. Al-Kandari, A.M. Mohamed, F. Al-Kharafi, M.I. Zaki, A. Katrib, Appl. Catal. A: Gen. 417–418 (2012) 298.
[46] H. Al-Kandari, A.M. Mohamed, S. Al-Kandari, F. Al-Kharafi, G.A. Mekhemer, M.I. Zaki, A. Katrib, J. Mol. Catal. A: Chem. 368–369 (2013) 1.
[47] T. Matsuda, T. Ohno, Y. Hiramatsu, Z. Li, H. Sakagami, N. Takahashi, Appl. Catal. A: Gen. 362 (2009) 40.
[48] T. Ohno, Z. Li, N. Sakai, H. Sakagami, N. Takahashi, T. Matsuda, Appl. Catal. A: Gen. 389 (2010) 52.